Journal of the European Ceramic Society 38 (2018) 4677–4681

Contents lists available at ScienceDirect

Journal of the European Ceramic Society

journal homepage: www.elsevier.com/locate/jeurceramsoc

Original article

A new series of low-temperature cofirable $Li_3Ba_2La_{3(1-x)}Y_{3x}(MoO_4)_8$ microwave dielectric ceramics

Ruzhong Zuo[a,*], Yudong Xu[a], Min Shi[a], Weiqiong Li[a], Liangguo He[b]

[a] Institute of Electro Ceramics & Devices, School of Materials Science and Engineering, Hefei University of Technology, Hefei, 230009, PR China
[b] School of Mechanical Engineering, Hefei University of Technology, Hefei, 230009, PR China

ARTICLE INFO

Keywords:
Microwave dielectrics ceramics
Low-temperature firing
LTCC
Molybdate

ABSTRACT

A new series of $Li_3Ba_2La_{3(1-x)}Y_{3x}(MoO_4)_8$ microwave dielectric ceramics were prepared by a conventional solid-state reaction method. The Rietveld refinement results further confirm that $Li_3Ba_2La_{3(1-x)}Y_{3x}(MoO_4)_8$ belongs to a monoclinic system with space group C2/c. Scanning electron microscopy results reveal that $Li_3Ba_2La_{3(1-x)}Y_{3x}(MoO_4)_8$ ceramics can be well sintered at a low sintering temperature. In addition, the permittivity (ε_r) of $Li_3Ba_2La_{3(1-x)}Y_{3x}(MoO_4)_8$ ceramics was found to decrease gradually with increasing substitution content of Y^{3+}, while the quality factor (Qxf) and temperature coefficient of resonant frequency (τ_f) increase with x monotonously. The x = 0.4 ceramic sintered at 700 °C for 4 h possesses optimum microwave dielectric properties of $\varepsilon_r \sim 14.4$, Qxf ~ 14,994 GHz (at 9.0 GHz) and $\tau_f \sim +6.9$ ppm/°C. Particularly, no chemical reaction between the matrix phase and Ag metal suggests that the $Li_3Ba_2La_{1.8}Y_{1.2}(MoO_4)_8$ ceramic might be a promising candidate for low-temperature co-fired ceramic applications.

1. Introduction

With the rapid development of wireless communication technology, high-performance microwave devices have been earnestly needed nowadays [1]. Particularly, the low temperature co-fired ceramic (LTCC) technology has attracted much attention due to its ability in the miniaturization and integration of microwave components. This technology has played an increasingly important role in the fabrication of modern electronic devices. It requires dielectric ceramics to have a low sintering temperature for cofiring with Ag, a low permittivity (ε_r) for avoiding the signal delay, a high quality factor (Qxf) for better selectivity and a low temperature coefficient of resonant frequency (τ_f) for the frequency stability [2].

Up to now, a great number of low-loss dielectric materials have been widely studied, such as $MgSiO_3$, Mg_2SiO_4, Zn_2SiO_4, $MgAl_2O_4$, but their high sintering temperatures have restricted their possible applications in LTCC [3–6]. The addition of some low-melting-point sintering aids was considered as a more common and effective method to reduce the sintering temperature of dielectric ceramics. However, microwave dielectric properties of the matrix ceramics were seriously degraded in most cases. Therefore, it is desirable to develop new material systems with excellent microwave dielectric properties and intrinsically low sintering temperatures. Recently, a mass of molybdate ceramic systems have attracted extensive attention for their good dielectric performances and extremely low sintering temperatures. For example, $Na_2Zn_5(MoO_4)_6$ ceramics sintered at 590 °C for 1 h present microwave dielectric properties of $\varepsilon_r \sim 8.1$ Qxf ~ 35,800 GHz and $\tau_f \sim -95$ ppm/°C [7]. $NaAgMoO_4$ sintered at an ultra-low temperature (about 400 °C) possesses dielectric properties of $\varepsilon_r \sim 7.9$, Qxf ~ 33,000 GHz and $\tau_f \sim -120$ ppm/ °C [8]. In our recent work, a series of molybdate ceramics $Ln_2Zr_3(MoO_4)_9$ (Ln = La, Sm, Nd) also exhibit excellent microwave dielectric properties of $\varepsilon_r = 10.8 \sim 11.0$, Qxf = 50,628 ~ 74,012 GHz and $\tau_f = -38.8 \sim -45.3$ ppm/°C at sintering temperatures of 775 °C–875 °C [9,10]. This would stimulate us to explore new Mo-based ceramic systems for meeting the demands of LTCC technology.

The monoclinic $Li_3Ba_2Ln_3(MoO_4)_8$ (Ln = La and Y) ceramic has been widely studied as excellent laser host materials [11–13]. Its crystal structure consists of five kinds of oxygen polyhedrons including La/Li/BaO_8 polyhedrons, Ba/LnO_{10} polyhedrons, LiO_6 octahedra and two types of MoO_4 tetrahedrons, in which the majority of Ba^{2+} ions and a small part of Ln^{3+} are coordinated by 10 oxygen anions, whereas the rest shares the same 8-fold coordinated site with Li^+ ions. Particularly, it can be synthesized at a low temperature, which prompts our interests in studying their microwave dielectric properties. In this work, a series of $Li_3Ba_2La_{3(1-x)}Y_{3x}(MoO_4)_8$ ($0 \le x \le 1.0$) ceramics were prepared by a conventional solid-state reaction method in order to achieve high-performance dielectric materials. The sintering behavior, phase composition, microstructures and microwave dielectric properties of the

---

* Corresponding author.
E-mail address: piezolab@hfut.edu.cn (R. Zuo).

https://doi.org/10.1016/j.jeurceramsoc.2018.06.019
Received 24 April 2018; Received in revised form 7 June 2018; Accepted 8 June 2018

ceramics were studied in detail.

2. Experimental

The $Li_3Ba_2La_{3(1-x)}Y_{3x}(MoO_4)_8$ ($0 \le x \le 1.0$) ceramics were synthesized using high-purity starting powders of analytic-grade Li_2CO_3, Ba_2CO_3, La_2O_3, Y_2O_3 and MoO_3. The raw materials were weighed in stoichiometric amounts and then ball-milled for 4 h using zirconia balls and alcohol as the medium on a planetary milling machine. The resulting slurries were then rapidly dried and calcined at 600 °C for 6 h in air. The calcined powders were re-milled for 6 h and then mixed together with 5 wt% PVA as a binder. The granulated powders were subsequently pressed into cylinders with dimensions of 10 mm in diameter and 7–8 mm in height. The specimens were first heated at 550 °C in air for 4 h to remove the organic binder, and then sintered at 650 °C ~ 750 °C for 4 h.

The crystal structure of the fired ceramics was identified via an X-ray diffractometer (XRD, D/Max2500 V, Rigaku, Japan) using CuK_α radiation. The structural parameters were obtained from Rietveld refinement of the XRD data using the GSAS-EXPGUI program. The bulk densities of the sintered ceramics were measured by the Archimedes method. The theoretical density (ρ_{th}) was calculated by using the structure refinement data. The microstructure of the specimens was observed using a field-emission scanning electron microscope (FE-SEM; SU8020, JEOL, Tokyo, Japan) equipped with an energy dispersive spectrometer (EDS). For the observation of grain morphology, the samples were polished and then thermally etched at 620 °C for 30 min. Microwave dielectric properties of the sintered ceramics were measured using a network analyzer (N5230C, Agilent, Palo Alto, CA) and a temperature chamber (GDW-100, Saiweisi, Changzhou, China). The τ_f values of the samples were measured in the temperature range of 20 ~ 80 °C and calculated by the following equation:

$$\tau_f = \frac{f_2 - f_1}{f_1 (T_2 - T_1)} \tag{1}$$

where f_1 and f_2 represent the resonant frequencies at T_1 and T_2, respectively.

3. Results and discussion

Fig. 1(a) presents the XRD patterns of $Li_3Ba_2La_{3(1-x)}Y_{3x}(MoO_4)_8$ ($0 \le x \le 1.0$) ceramics sintered at 700 °C for 4 h. All of the diffraction peaks match well with the standard JCPDS file 77-0830 and no secondary phase can be detected, indicating the formation of pure-phase ceramics. In addition, it should be noted that the main diffraction peaks slightly shift to higher angles with increasing x, as plotted in Fig. 1(b), meaning that the cell volume decreases with the increase of x due to the substitution of smaller Y^{3+} ions for larger La^{3+} in the $Li_3Ba_2La_{3(1-x)}Y_{3x}(MoO_4)_8$ ceramics. In order to understand its structure in details, Rietveld refinements were carried out by using GSAS software, in which a structural model of $Li_3Ba_2Gd_3(MoO_4)_8$ was used [11]. The refined plot of the x = 0.4 sample sintered at 700 °C was selected as a representative, as shown in Fig. 2. The lattice parameters, cell volume and reliability factors of R_{wp}, R_p, and χ^2 for all studied samples sintered at their optimum sintering temperatures are listed in Table 1, in which R_{wp} is the reliability factor of weighted patterns, R_p is the reliability factor of patterns and χ^2 is the goodness-of-fit indicator ($(R_{wp}/R_{exp})^2$). The R_{wp}, R_p, and χ^2 values were found to be in the range of 6.6–8.3%, 5.2–6.6%, and 1.5–2.0, respectively, indicating that the structural model is valid and the refinement result is reliable. Moreover, these crystal structure parameters are similar to those in a previous report [13]. It is obvious that the substitution of Y^{3+} for La^{3+} can lead to a decrease in lattice parameter and unit cell volume. According to the unit cell volume, the ρ_{th} value of each sample can be then obtained, as listed in Table 1.

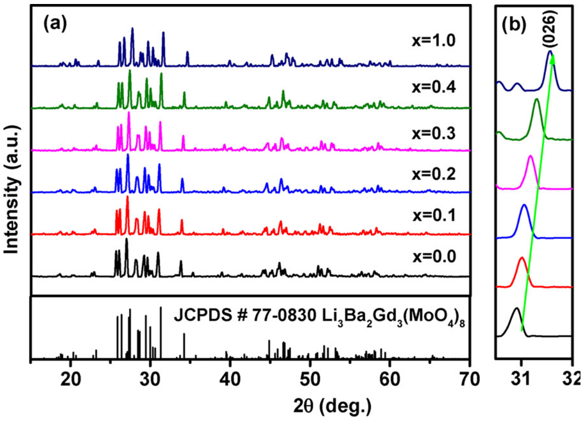

Fig. 1. XRD patterns of $Li_3Ba_2La_{3(1-x)}Y_{3x}(MoO_4)_8$ ($0 \le x \le 1$) ceramics sintered at 700 °C for 4 h.

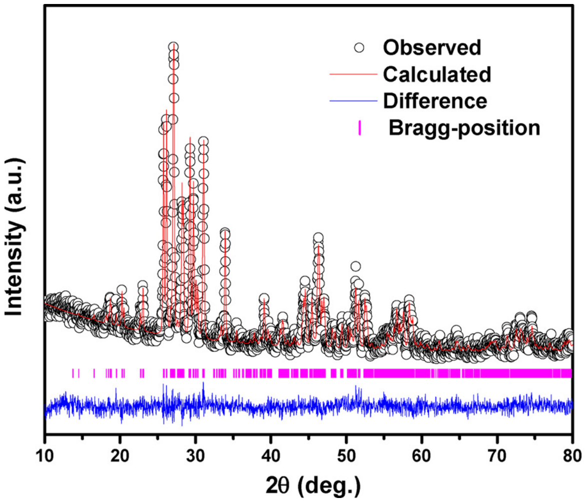

Fig. 2. The Rietveld refinement plot of the x = 0.4 sample sintered at 700 °C for 4 h.

Fig. 3 shows the SEM images on polished and thermally etched surfaces of $Li_3Ba_2La_{3(1-x)}Y_{3x}(MoO_4)_8$ ($0.0 \le x \le 1.0$) ceramics sintered at 700 °C for 4 h. All the studied samples exhibit dense microstructure with identifiable grain boundaries. This is consistent with the measurement of the Archimedes density (< 95% for all samples, see infra). The average grain size of the samples was found to gradually increase with increasing x values.

Fig. 4 shows the variation of relative density, ε_r and Qxf values of $Li_3Ba_2La_{3(1-x)}Y_{3x}(MoO_4)_8$ ($0 \le x \le 1$) ceramics as a function of sintering temperature. As shown in Fig. 4(a), with increasing sintering temperature, the relative densities of all studied samples firstly increase to their respective maximum values approximately at 700 °C, and then decrease with further increasing sintering temperature. Each composition possesses high relative densities (> 95%) at the optimum temperature. The ε_r values of $Li_3Ba_2La_{3(1-x)}Y_{3x}(MoO_4)_8$ ($0 \le x \le 1.0$) ceramics changing with x (Fig. 4(b)) presents a similar variation trend with density, indicating density might be a primary affecting factor of ε_r in this work. In addition, the ε_r values of the $Li_3Ba_2La_{3(1-x)}Y_{3x}(MoO_4)_8$ ($0 \le x \le 1.0$) ceramics decrease with increasing x values as a result of reduced relative densities at the optimum sintering temperature. It is well known that the dielectric loss should involve extrinsic loss and intrinsic loss. The variation of Qxf values of $Li_3Ba_2La_{3(1-x)}Y_{3x}(MoO_4)_8$ ($0 \le x \le 1$) ceramics (Fig. 4(c)) as a function of sintering temperature can be mainly attributed to the extrinsic loss caused by density, grain size and lattice defects, etc. Considering all compositions possess high relative densities, the structure characteristics should dominate

Table 1
Refined unit cell volume, theoretical density, reliability factors and good-of-fit indicator of $Li_3Ba_2La_{3(1-x)}Y_{3x}(MoO_4)_8$ ($0 \le x \le 1.0$) ceramics sintered at 700 °C for 4 h.

Composition	a (Å)	b (Å)	c (Å)	Unit cell volume (Å^3)	ρ_{th} (g/cm^3)	R_{wp} (%)	R_p (%)	χ^2
x = 0.0	5.0382(2)	12.9976(5)	19.360(8)	1335.6(1)	4.952	8.28	6.51	1.92
x = 0.2	5.2892(4)	12.9324(9)	19.291(1)	1319.3(2)	4.938	7.14	5.66	1.52
x = 0.3	5.2801(3)	12.9072(7)	19.268(1)	1313.0(1)	4.924	7.16	5.65	1.51
x = 0.4	5.2677(3)	12.8681(8)	19.227(1)	1303.2(2)	4.922	6.80	5.34	1.51
x = 0.5	5.2583(5)	12.8395(1)	19.203(1)	1296.2(2)	4.912	6.99	5.56	1.53
x=1.0	5.1942(3)	12.6661(7)	19.067(1)	1254.1(2)	4.878	6.63	5.27	1.60

different Qxf values between them, as evaluated by the packing fraction (f). It can be defined by the sum of the volume of packed ions (V_{PI}) over the volume of a primitive unit cell (V_{PUC}), as expressed by the following equation [14]:

$$f\,(\%) = \frac{V_{PI}}{V_{PUC}} xZ \tag{2}$$

where Z is the number of molecule per unit cell. The dependence of Qxf values on the packing fraction is clearly shown in Fig. 5(a). As expected, the Qxf values of the ceramics increase with increasing packing fraction values, which should correspond to the increased substitution amount of Y^{3+} for La^{3+}.

Except for ε_r and Qxf, the τ_f value is another important dielectric property for the GHz application, which determines the thermal stability of materials and devices. The τ_f value of a material is related to the chemical nature of constituent ions, the distance between cations and anions, and the structural characteristics originating from the bonding type, as evaluated by the bond valence of ions (V_i) defined as the sum of all of the valences from a given atom i, as expressed by the following equation [14,15]:

$$\nu_i = \sum_j \nu_{ij} \tag{3}$$

$$\nu_{ij} = \exp\left\{\frac{(R_{ij} - d_{ij})}{b}\right\} \tag{4}$$

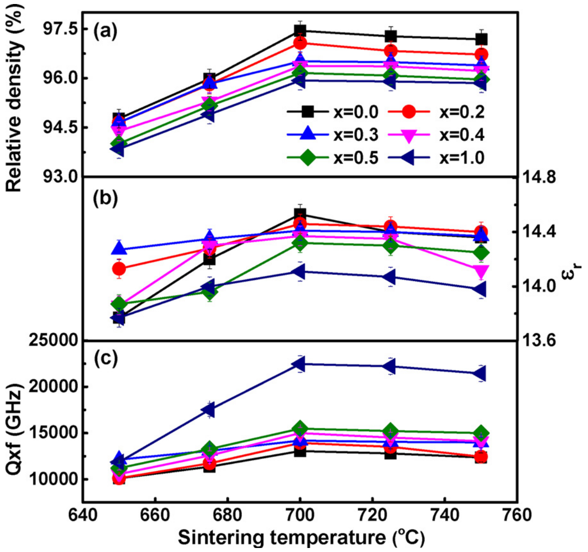

Fig. 4. The variation of (a) relative density, (b) ε_r and (c) Qxf of $Li_3Ba_2La_{3(1-x)}Y_{3x}(MoO_4)_8$ ($0 \le x \le 1$) ceramics as a function of sintering temperature.

where R_{ij} is the bond valence parameter, d_{ij} is the length of a bond between atoms i and j, and b is commonly taken to be a universal constant equal to 0.37 Å. Bond valence is a weighted average according to the occupancy of each cation at its specific site. Therefore, an appropriate understanding of the coordination condition of the Ln site would be necessary in current ceramic systems. As mentioned previously, there are two kinds of La^{3+}/ Y^{3+} ions in the Ln site. The

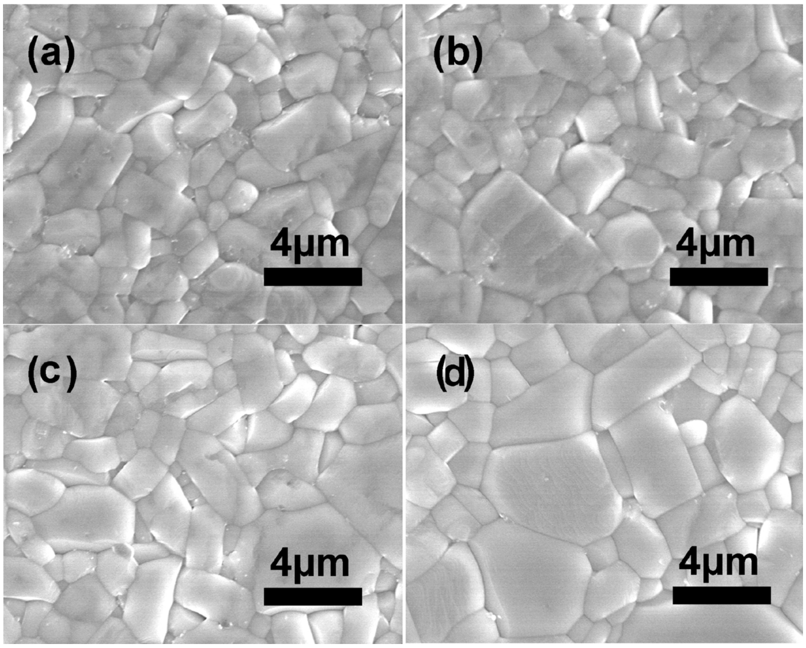

Fig. 3. SEM images of $Li_3Ba_2La_{3(1-x)}Y_{3x}(MoO_4)_8$ ($0 \le x \le 1$) ceramics sintered at 700 °C for 4 h: (a) x = 0, (b) x = 0.2, (c) x = 0.4 and (d) x = 1.0.

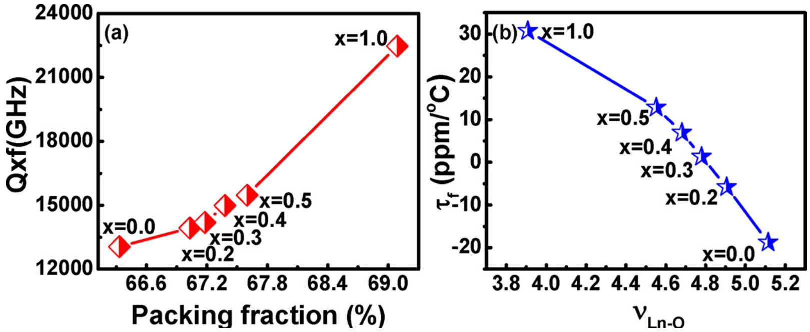

Fig. 5. (a) The variation of Qxf against the packing fraction, and (b) the τ_f value against the Ln-site bond valence for $Li_3Ba_2La_{3(1-x)}Y_{3x}(MoO_4)_8$ ($0 \le x \le 1$) ceramics.

Table 2
The bond valence of $Li_3Ba_2La_{3(1-x)}Y_{3x}(MoO_4)_8$ ($0 \le x \le 1.0$) ceramics sintered at 700 °C for 4 h.

Composition	$V_{La1\text{-}O}$	$V_{Y1\text{-}O}$	$V_{La2\text{-}O}$	$V_{Y2\text{-}O}$	$V_{Ln\text{-}O}$
x = 0.0	1.518	0.995	3.596	2.378	5.115
x = 0.2	1.568	1.029	3.696	2.444	4.906
x = 0.3	1.588	1.042	3.735	2.470	4.780
x = 0.4	1.620	1.062	3.798	2.511	4.681
x = 0.5	1.643	1.077	3.843	2.541	4.552
x = 1.0	1.790	1.174	4.132	2.732	3.907

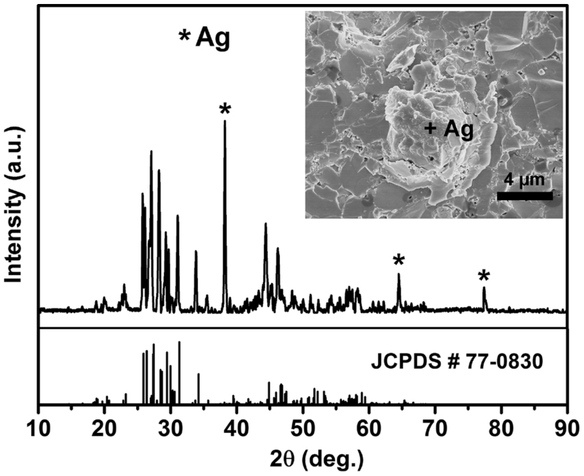

Fig. 6. The XRD patterns of the cofired sample of the x = 0.4 powder and 30 wt % Ag; the inset shows the SEM graph on the fractured surface of the cofired sample.

majority of La^{3+}/Y^{3+} ions (La2/Y2) occupy the site with 8-fold coordination, and the remaining small percentage of La^{3+}/Y^{3+} ions (La1/Y1) occupy the site with 10-fold coordination, so the bond valence of the Ln site can be calculated as follows:

$$V_{Ln\text{-}O} = (1\text{-}x)\ [w_{La1}V_{La1\text{-}O} + w_{La2}V_{La2\text{-}O}] + x[w_{Y1}V_{Y1\text{-}O} + w_{Y2}V_{Y2\text{-}O}] \tag{5}$$

where $V_{Ln\text{-}O}$ is the sum of all the valences from the cations in the Ln site, $w_{La/Y}$ is the occupying mole fraction of the La^{3+}/Y^{3+} cations in the two different coordination, and x is the mole fraction of Y^{3+} cations in the $Li_3Ba_2La_{3(1-x)}Y_{3x}(MoO_4)_8$ ceramics. The details of Ln-site bond valences in $Li_3Ba_2La_{3(1-x)}Y_{3x}(MoO_4)_8$ ceramics are presented in Table 2. The variation of the τ_f value in $Li_3Ba_2La_{3(1-x)}Y_{3x}(MoO_4)_8$ samples as a function of the Ln-site bond valence is shown in Fig. 5(b). With an increase of Y^{3+} contents, the Ln-site bond valence gradually decreases, while the τ_f value increases monotonously. Actually, it has been proved in complex perovskites that the decrease of B-site bond valence would result in the increase of τ_f [16,17]. In current work, the substitution of smaller Y^{3+} ions for bigger La^{3+} ions tends to increase the restoring force for recovering the tilting of polyhedron. As a result, τ_f undergoes a considerable change from negative to positive values.

In order to identify the suitability of LTCC applications, the chemical compatibility of the ceramic with Ag was examined. 30 wt% Ag powder was added into the x = 0.4 powder, and the mixture was sintered at 700 °C for 4 h. Fig. 6 shows the XRD patterns and of the co-fired sample at 700 °C. It is noted that all diffraction peaks can be well indexed to a standard JCPDS file 77-0830 ($Li_3Ba_2Gd_3(MoO_4)_8$) and a standard JCPDS file 87-0597 (Ag), indicating that no any chemical reaction occurs between the ceramic and the Ag particle. This can be further confirmed by the SEM and the EDS result of the cofired sample, as shown in the inset image of Fig. 6. The grain boundary between the ceramic and the Ag particle can be distinctly distinguished. The large bright particle can prove to be Ag through the EDS result. These results demonstrate an excellent chemical stability between the $Li_3Ba_2La_{1.8}Y_{1.2}(MoO_4)_8$ ceramic and the Ag metal at 700 °C and a large potential of the studied ceramic for LTCC applications.

4. Conclusions

In this work, a series of new microwave dielectric ceramics $Li_3Ba_2La_{3(1-x)}Y_{3x}(MoO_4)_8$ were successfully synthesized by a conventional solid-state method. A continuous single-phase solid solution ceramic between $Li_3Ba_2La_3(MoO_4)_8$ and $Li_3Ba_2Y_3(MoO_4)_8$ can be formed in the whole composition range. All the studied samples exhibit dense microstructures with high relative densities. The substitution of Y^{3+} for La^{3+} in $Li_3Ba_2La_{3(1-x)}Y_{3x}(MoO_4)_8$ ceramics can induce the lattice distortion, leading to the change of the τ_f from negative to positive values. In the meantime, the ε_r value of the ceramics gradually decreases, while the Qxf values increase monotonously. The optimum microwave dielectric properties of $\varepsilon_r = 14.4$, $Q \times f = 14{,}994$ GHz (9.4 Hz), and $\tau_f = 6.9$ ppm/°C are obtained in the x = 0.4 composition as sintered at 700 °C for 4 h. Besides, the $Li_3Ba_2La_{1.8}Y_{1.2}(MoO_4)_8$ ceramic exhibits a good chemical compatibility with Ag, showing a large potential in the application of LTCC technology.

Acknowledgements

This work was financially supported by the Special Funds for Science and Technology Development of Guangdong Province (Grant No. 2017A010101001).

References

[1] M.T. Sebastian, H. Jantunen, Low loss dielectric materials for LTCC applications: a review, Int. Mater. Rev. 53 (2008) 57–90.
[2] M. Valant, D. Suvorov, Chemical compatibility between silver electrodes and low-firing binary-oxide compounds: conceptual study, J. Am. Ceram. Soc. 83 (2000) 2721–2729.
[3] M.E. Song, J.S. Kim, M.R. Joung, S. Nahm, Y.S. Kim, J.H. Paik, B.H. Choi, Synthesis and microwave dielectric properties of $MgSiO_3$ ceramics, J. Am. Ceram. Soc. 91 (2008) 2747–2750.

[4] T. Tsunooka, M. Androu, Y. Higashida, H. Sugiura, H. Ohsato, Effects of TiO_2 on sinterability and dielectric properties of high-Q forsterite ceramics, J. Eur. Ceram. Soc. 23 (2003) 2573–2578.

[5] Y.P. Guo, H. Ohsato, K. Kakimoto, Characterization and dielectric behavior of willemite and TiO_2-doped willemite ceramics at millimeter-wave frequency, J. Eur. Ceram. Soc. 26 (2006) 1827–1830.

[6] A. Kan, H. Ogawa, A. Yokoi, Y. Nakamura, Crystal structural refinement of corundum-structured $A_4M_2O_9$ (A = Co and Mg, M = Nb and Ta) microwave dielectric ceramics by high-temperature x-ray powder diffraction, J. Eur. Ceram. Soc. 27 (2007) 2977–2981.

[7] J. Dhanya, A.V. Basiluddeen, R. Ratheesh, Synthesis of ultra-low temperature sinterable $Na_2Zn_5(MoO_4)_6$ ceramics and the effect of microstructure on microwave dielectric properties, Scr. Mater. 132 (2017) 1–4.

[8] D. Zhou, L.X. Pang, Z.M. Qi, B.B. Jin, X. Yao, Novel ultra-low temperature co-fired microwave dielectric ceramic at 400 degrees and its chemical compatibility with base metal, Sci. Rep. 4 (2014) 5980.

[9] W. Liu, R.Z. Zuo, A novel low-temperature firable $La_2Zr_3(MoO_4)_9$ microwave dielectric ceramic, J. Eur. Ceram. Soc. 38 (2018) 339–342.

[10] W. Liu, R.Z. Zuo, Low temperature fired $Ln_2Zr_3(MoO_4)_9$ (Ln = Sm, Nd) microwave dielectric ceramics, Ceram. Int. 43 (2017) 17229–17232.

[11] A. Katelnikovas, J. Plewa, S. Sakirzanovas, D. Dutczak, D. Enseling, F. Baur, H. Winkler, A. Kareiva, T. Jüstel, Synthesis and optical properties of $Li_3Ba_2La_3(MoO_4)_8$: Eu^{3+} powders and ceramics for pcLEDs, J. Mater. Chem. 22 (2012) 22126–22134.

[12] M. Song, G. Wang, Z. Lin, L.Z. Zhang, G.F. Wang, Growth and spectral properties of Nd^{3+}-doped $Li_3Ba_2Y_3(MoO_4)_8$ crystal, J. Cryst. Growth 308 (2007) 208–212.

[13] C.F. Guo, F. Gao, L. Liang, B.C. Choi, J.H. Jeong, Synthesis, characterization and luminescent properties of novel red emitting phosphor $Li_3Ba_2Ln_3(MoO_4)_8$: Eu^{3+}(Ln = La, Gd and Y) for white light-emitting diodes, J. Alloys Compd. 479 (2009) 607–612.

[14] E.S. Kim, B.S. Chun, R. Freer, R.J. Cernik, Effects of packing fraction and bond valence on microwave dielectric properties of $A^{2+}B^{6+}O_4$ (A^{2+}: Ca, Pb, Ba; B^{6+}: Mo, W) ceramics, J. Eur. Ceram. Soc. 30 (2010) 1731–1736.

[15] J. Zhang, R.Z. Zuo, Effect of ordering on the microwave dielectric properties of spinel- structured $(Zn_{1-x}(Li_{2/3}Ti_{1/3})_x)_2TiO_4$ ceramics, J. Am. Ceram. Soc. 99 (2016) 3343–3349.

[16] H.S. Park, K.H. Yoon, E.S. Kim, Effect of bond valence on microwave dielectric properties of complex perovskite ceramics, Mater. Chem. Phys. 79 (2003) 181–183.

[17] Q. Liao, L. Li, P. Zhang, L. Cao, Y. Han, Correlation of crystal structure and microwave dielectric properties for $ZnTi(Nb_{1-x}Ta_x)_2O_8$ ceramics, Solid State Sci. 13 (2011) 1201–1204.